Structure-Guided Peptidomimetic Design Leads to Nanomolar β-Hairpin Inhibitors of the Tat−TAR Interaction of Bovine Immunodeficiency Virus[†,‡]

Zafiria Athanassiou,[§] Krystyna Patora,[||] Ricardo L. A. Dias,[||] Kerstin Moehle,[||] John A. Robinson,*[,||] and Gabriele Varani*[,§,⊥]

Department of Chemistry and Department of Biochemistry, University of Washington, Seattle, Washington 98195, and Department of Chemistry, University of Zurich, Winterthurerstrasse 190, 8057 Zurich, Switzerland

Received September 18, 2006; Revised Manuscript Received November 7, 2006

ABSTRACT: The Tat protein of immunodeficiency viruses is the main activator of viral gene expression. By binding specifically to its cognate site, the transactivator response element (TAR), Tat mediates a strong induction of the production of all viral transcripts. In seeking a new chemical solution to inhibiting viral protein−RNA interactions, we recently identified inhibitors of the viral Tat protein from the bovine immunodeficiency virus (BIV) using conformationally constrained β-hairpin peptidomimetics. We identified a micromolar ligand, called BIV2, and the structure of its complex with BIV TAR was determined by NMR. In this work, we demonstrate that this chemistry can rapidly yield highly potent and selective ligands. On the basis of the structure, we synthesized and assayed libraries of mutant peptidomimetics. Remarkably, we were able in just a few rounds of design and synthesis to discover nanomolar inhibitors of the Tat−TAR interaction in BIV that selectively bind the BIV TAR RNA compared to RNA structures as closely related as the HIV-1 TAR or RRE elements. The molecular recognition principles developed in this study have been exploited in discovering related peptidomimetic inhibitors of the Tat−TAR interaction in HIV-1.

The growing awareness of the involvement of RNA in the progression of disease makes the discovery of new RNA-binding molecules for treating infectious and chronic diseases an important challenge (*1*). Two fundamental approaches exist. First, oligonucleotides can be targeted to specific RNA sequences not involved in stable secondary structures; gene expression can then be repressed by antisense or RNAi[1] mechanisms. However, there remain considerable limitations with regard to both pharmacology and cost before these technologies can be brought routinely to clinical use, despite significant recent progress with regard to new oligonucleotide chemistry (*2*−*5*). Second, small molecule ligands can be targeted to highly structured RNAs (for example, riboswitches or protein-binding sites) to inhibit the function of RNA regulatory elements of bacterial or viral origin. The complexity and diversity of RNA structures offer attractive targets for the design of small molecule ligands to be used as pharmacological agents (*6*, *7*), but the discovery of compounds capable of binding to RNA specifically and with high potency remains very challenging.

Among the most studied RNA targets for the treatment of infectious diseases are the RNA regulatory elements from HIV-1 and related lentiviruses. Two protein−RNA complexes encoded by these viruses, Rev−RRE and Tat−TAR, regulate viral gene expression and represent very attractive candidates for intervention. Tat protein is the main activator of viral gene expression. By specifically binding to the TAR RNA element, it mediates a strong induction of the production of all viral transcripts by boosting the efficiency of the cellular polymerase (*8*). The Tat−TAR complex recruits two cellular cofactors, cyclin T1 and its cognate kinase CDK9, that stimulate transcriptional elongation from the viral long terminal repeat (LTR) (*9*). Agents that disrupt the Tat−TAR interaction block the production of full-length transcripts and reduce HIV-1 replication rates (*10*−*12*). If binding of Tat to TAR could be disrupted specifically, the resultant transcriptional block would be HIV-1 specific, because there is no cellular counterpart to Tat or TAR. Furthermore, inhibition of Tat would be effective not only for infected cells that are actively replicating but also for infected cells in latency, because Tat protein is required for reactivation of viral production in latent cells (*13*, *14*).

[†] This work was supported by NIH Grant AI 60410 to G.V. and a NSF grant to J.A.R.

[‡] The structures have been deposited in the Protein Data Bank as entry 2NS4.

* To whom correspondence should be addressed. G.V.: e-mail, varani@chem.washington.edu; phone, (206) 543-7113; fax, (206) 685-8665. J.A.R.: e-mail, robinson@oci.unizh.ch; phone, +44-6354242; fax, +446356833.

[§] Department of Chemistry, University of Washington.

[||] University of Zurich.

[⊥] Department of Biochemistry, University of Washington.

[1] Abbreviations: HIV, human immunodeficiency virus; TAR, transactivation response region; BIV, bovine immunodeficiency virus; RRE, Rev response element; RNAi, ribonucleic acid interference; LTR, long terminal repeat; PAGE, polyacrylamide gel electrophoresis; CDK9, cyclin-dependent kinase 9; NMR, nuclear magnetic resonance; DQF-COSY, double-quantum-filtered correlation spectroscopy; TOCSY, total correlation spectroscopy; NOESY, nuclear Overhauser effect spectroscopy; NOE, nuclear Overhauser effect; DMF, *N*,*N*-dimethylformamide; Fmoc, 9-fluorenylmethoxycarbonyl; HATU, 2-(1*H*-9-azabenzotriazol-1-yl)-1,1,3,3-tetramethyluronium hexafluorophosphate; HOAt, *N*-hydroxy-9-azabenzotriazole; TIPS, triisopropylsilane; TFA, trifluoroacetic acid.

10.1021/bi0619371 CCC: $37.00
Published on Web 12/21/2006

Given the important role of Tat in HIV-1 replication, significant efforts have been dedicated to discovering molecules capable of binding to TAR and of inhibiting Tat-dependent transactivation, but so far, no suitable clinical candidates have been found (*15*). In an effort to discover new chemical solutions to the problem of targeting RNA structures, we have considered peptidomimetic chemistry that has received considerable attention recently for the inhibition of protein−protein complexes (*16*, *17*). As in that case, we reasoned that peptidomimetics that target specific RNA structures could provide novel molecular entities for controling cellular processes involving protein−RNA complexes (*18*). On the basis of this rationale, we recently sought inhibitors of the Tat protein using peptidomimetic chemistry and a structure-based approach (*19*). Since structural information about the HIV Tat−TAR complex is not yet available (*20*−*22*), we decided to use the corresponding interaction from BIV to study the chemistry and molecular recognition principles concerning TAR recognition by structurally and conformationally constrained peptidomimetics. This second lentivirus uses a very similar mechanism of transcriptional activation to HIV, and the structure and sequence of their TAR and Tat elements are particularly similar to each other. Most importantly, the three-dimensional structure of BIV TAR in a complex with a Tat-derived peptide has been determined (*23*, *24*), revealing that BIV Tat forms a β-hairpin conformation in complex with BIV TAR. We reasoned that the HIV Tat−TAR system could be mimicked by the BIV complex for the purpose of inhibitor design, and we sought to discover conformationally constrained β-hairpin mimetics of BIV Tat protein. Moreover, we anticipated that the information derived from the bovine virus could be exported, at least in part, to the human virus, as indeed has been the case (Z. Athanassiou et al., manuscript in preparation).

We previously reported the design, synthesis, and analysis of a small family of β-hairpin peptidomimetics that included a relatively potent inhibitor of the BIV Tat−TAR complex called BIV2 that formed a stable β-hairpin structure in solution (Figure 1) (*19*). The preorganization of BIV2 into a β-hairpin allowed us to determine the structure of this new RNA ligand in its complex with BIV TAR (*25*). We found that BIV2 induces a conformational change in the RNA leading to a structure that is very similar to that of Tat-bound BIV TAR (Figure 2). However, we were surprised to discover that BIV2 was bound to TAR in an orientation that is flipped head to tail by 180° compared to that expected on the basis of the BIV Tat−TAR structure yet retained key intermolecular contacts that direct the RNA conformational change. In this study, we use the structure of the BIV2−RNA complex to guide the design of new generation peptidomimetic libraries and gain insight into the origins of affinity and specificity of this ligand−RNA interaction. Through just a few cycles of design and assay, we have identified new nanomolar inhibitors of the BIV Tat−TAR interaction that are also highly specific.

MATERIALS AND METHODS

Peptide Synthesis. The wild-type BIV Tat peptide (residues 65−81 with a C-terminal amide, Ac-SGPRPRGTRGKGR-RIRR-NH_2) was prepared on MBHA-Rink amide resin using Fmoc chemistry on an Applied Biosystems 433A peptide synthesizer. The concentrations of peptides were determined by UV absorbance (280 nm, for peptides containing Tyr) (*26*) or by quantitative amino acid analysis.

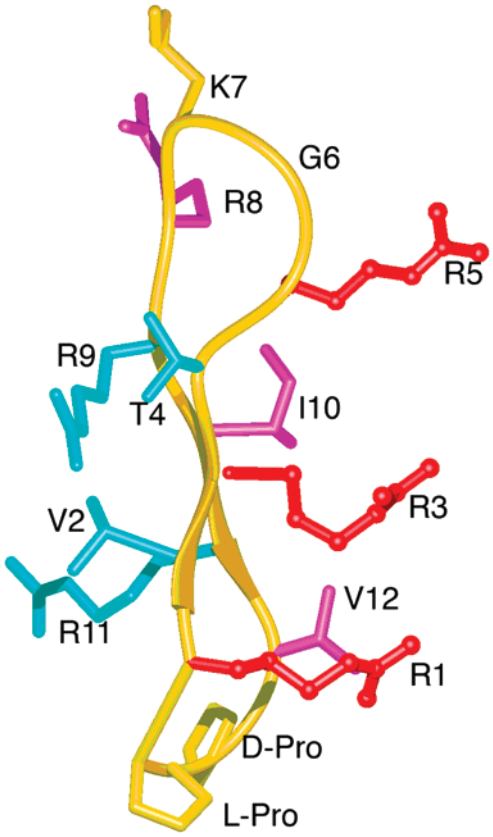

FIGURE 1: β-Hairpin structure of BIV2 [cyclo-(D-Pro-L-Pro-Arg^1-Val^2-Arg^3-Thr^4-Arg^5-Gly^6-Lys^7-Arg^8-Arg^9-Ile^{10}-Arg^{11}-Val^{12})] bound to BIV TAR RNA. Side chains at positions 1, 3, 5, 8, 10, and 12 interact with the major groove of the RNA, whereas residues 2, 4, 9, and 11 are on the face exposed to the solvent. Residues 6 and 7 at the tip of the BIV2 β-hairpin point toward the tip of the RNA (see Figure 2). The β-hairpin-stabilizing D-Pro-L-Pro template is at the bottom.

The synthesis of cyclic peptides followed a two-step procedure, as outlined previously (*19*). Briefly, linear peptides were synthesized in parallel on a MultiSynTech Syro peptide synthesizer using Fmoc chemistry (*27*) and 2-chlorotrityl chloride resin (loading 0.5 mmol/g). Each Fmoc deprotection and coupling step was carried out twice to optimize the purity of the linear products. After cleavage from the resin with 0.8% TFA in CH_2Cl_2, each linear peptide was cyclized in DMF using a HATU/HOAt mixture (3 equiv) and diisopropylethylamine (6 equiv). After DMF removal, the protected cyclic peptides were treated with a TFA/TIPS/H_2O mixture (95/2.5/2.5) at room temperature for 4 h to remove side chain protecting groups. Precipitation with cold diethyl ether and purification by reverse phase HPLC (C_{18} column, gradient from 10 to 60% MeCN in H_2O with 0.1% TFA) gave pure peptidomimetics in typically 20−60% yields, and of >95% purity as judged by analytical HPLC and HPLC−MS (see the Supporting Information). Selected mimetics were also analyzed by high-field NMR spectroscopy (600 MHz). For several mimetics, ^{1}H NMR spectra were fully assigned and solution NMR structures were calculated (see below).

RNA Preparation and Gel Shift Assays. BIV TAR RNA was prepared by in vitro transcription using T7 RNA polymerase and synthetic oligonucleotide templates (*28*). The RNA oligonucleotides were purified by denaturing poly-

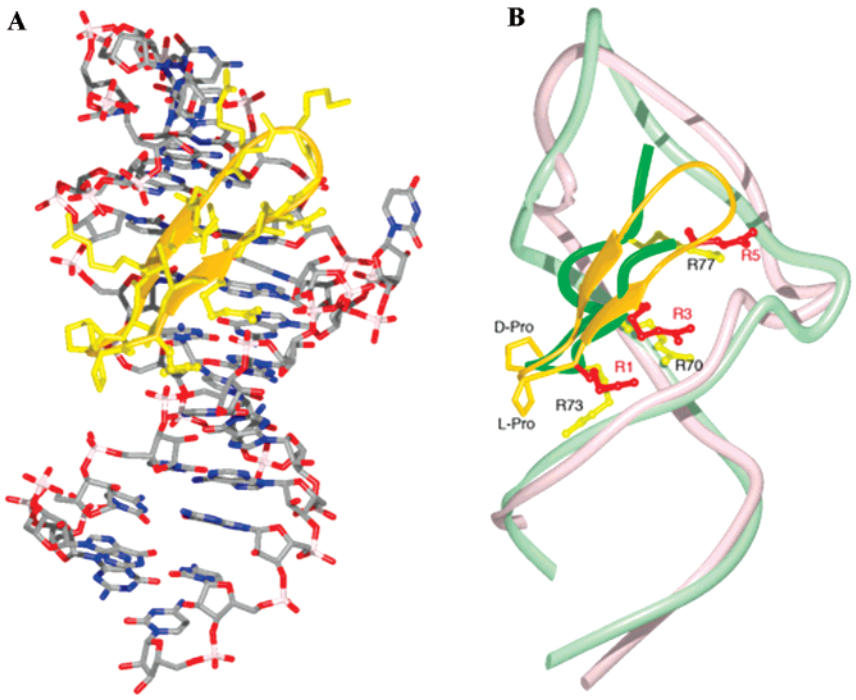

FIGURE 2: (A) Structure of the BIV2−TAR RNA complex and (B) superimposed ribbon diagrams of the BIV TAR−Tat complex (PDB entry 1MNB) (green) and the BIV TAR−BIV2 complex (PDB entry 2A9X) (pink and orange). Three key Arg residues in Tat (Arg70, Arg73, and Arg77) are colored yellow and in BIV2 (Arg3, Arg1, and Arg5) are colored red.

acrylamide gel electrophoresis (PAGE), and RNA concentrations were determined by the UV absorbance at 260 nm. ^{32}P-labeled BIV TAR RNA was prepared by 3′-end labeling using cytidine 3′,5′-bis[α-^{32}P]phosphate triethylammonium salt (pCp) and T4 RNA ligase (New England Biolabs). BIV TAR (30 pmol) was mixed with pCp (30 pmol), ATP (1 mM), T4 RNA ligase, bovine serum albumin (BSA), and T4 RNA ligase buffer and incubated at 37 °C for 18 h. The ligation mixture was passed through a desalting column, and the labeled BIV TAR was diluted to a final concentration of 20 nM. Binding assays were performed at 4 °C. Peptide and RNA were incubated in a buffer (10 μL) containing Tris-HCl (50 mM, pH 8.0), KCl (50 mM), DTT (200 mM), tRNA (*Escherichia coli*, 280 μg/μL), and Triton X-100 (0.05%). The samples were fractionated by being loaded onto 12% native polyacrylamide gels in 0.5% TB buffer and electrophoresed at 15 W and 4 °C. Dried gels were exposed to a phosphor imaging plate and scanned with a Molecular Dynamics phosphor imager. Bands corresponding to free and bound RNA were quantified using ImageQuant.

NMR Spectroscopy. ^{1}H NMR spectra were recorded on a Bruker DRX-600 spectrometer at typical peptide concentrations of 10−20 mg/mL in a 9/1 H_2O/D_2O mixture (pH 2.3) at 300 K. Water suppression was achieved by presaturation. ^{1}H NMR spectra were fully assigned using a combination of two-dimensional DQF-COSY, TOCSY, and NOESY data sets. Distance restraints were obtained from NOESY with mixing times of 250 ms. Additional NOESY spectra were recorded on peptide samples in 100% D_2O at 278 K to resolve CαH−CαH NOE cross-peaks close to the water signal. Spectra were typically collected with 1024 × 256 complex data points, zero-filled prior to Fourier transformation to 2048 × 1024 points, and transformed with a cosine-bell weighting function. Data processing was carried out with XWINNMR (Bruker) and XEASY (*29*).

Structure calculations were performed by restrained molecular dynamics in torsion angle space by applying the simulated annealing protocol implemented in DYANA (*30*). Starting from 100 randomized conformations, we selected a bundle of 20 conformations on the basis of the lowest DYANA target energy function. MOLMOL (*31*) was used for structure analysis and visualization of the calculated averaged structure models.

RESULTS

Peptidomimetic Synthesis. The BIV Tat mimetics were synthesized by first assembling a linear peptide chain on 2-chlorotrityl chloride resin, as described previously (*19*). The linear precursors were cleaved from the resin without removing the side chain protecting groups. Macrocyclization was then performed in a dilute DMF solution. The side chain protecting groups were removed with TFA, and the products were purified by reverse phase HPLC. In a typical synthesis, the main component in the crude product was the desired BIV mimetic. After purification by HPLC, the desired peptidomimetics were typically obtained in 20−60% overall yield, and each was >95% pure as determined by analytical HPLC and gave electrospray MS data consistent with the calculated masses (see the Supporting Information).

Design and Assay of New Peptidomimetics. To provide a control for the effect of cyclizing the peptide, we used the wild-type linear peptide BIV Tat(65−81) as a control in all binding studies. The K_d of this peptide determined by electrophoretic mobility shift assays (EMSAs) in the presence of a large (10000-fold) excess of tRNA was found to be 50 nM. In the same assay, BIV2 was found previously to have a K_d of 150 nM (Figure 3) (*19*).

To optimize the potency of the new peptidomimetic structures, we first changed each position in BIV2, except Gly6, to Ala to identify amino acid side chains that contribute

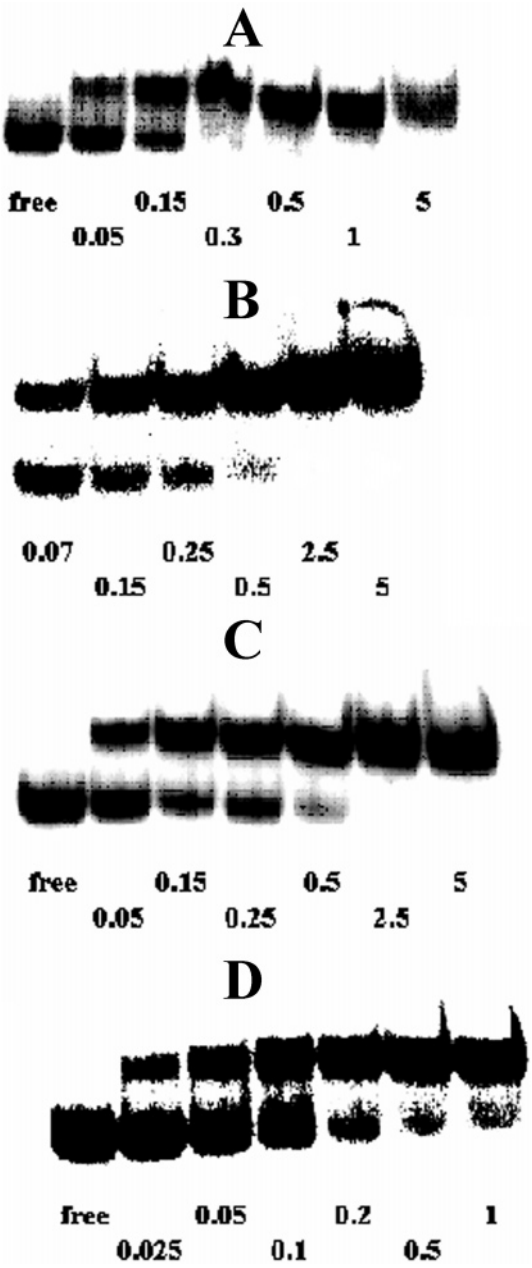

FIGURE 3: Binding of various peptidomimetics to BIV TAR (concentration of 1 nM) in the presence of a 10000-fold tRNA excess: (A) BIV2, (B) L-46, (C) L-51, and (D) L-57. Peptide concentrations are in micromolar.

significantly to the free energy of binding. Eleven new peptidomimetics, called BIV2-1−BIV2-12 (Table 1), were produced and assayed. The Ala mutants BIV2-12 and BIV2-10 were found to possess binding affinities in the low micromolar range, while the Ala mutants BIV2-2 and BIV2-4 bind to BIV TAR with an activity reduced only 2-fold compared to that of BIV2. No other Ala mutants exhibited binding to BIV TAR at the concentrations that were tested (micromolar).

In the next step, all positions in the RNA-contacting face of BIV2 were mutated in an effort to identify alternative side chains that would provide optimal contacts to the RNA. Arg residues that were found from the structure to have hydrogen bonding interactions with TAR were mutated to other charged residues, to distinguish between the requirements for hydrogen bonding and electrostatic interactions at each position. Hydrophobic residues (as found at positions 10 and 12) were mutated to other hydrophobic or charged residues in an effort to optimize the intermolecular contacts at these positions. Positions 2, 4, 9, and 11 on the solvent-exposed face (Figure 1) were also mutated in an effort to further increase the affinity by indirect conformational effects and to reduce the overall charge of the peptide. Finally, mutations were also introduced into multiple positions around the β-turn, to evaluate whether the energetic changes seen with single mutations were additive. The sequences of the mutants and their affinities for TAR RNA determined by EMSAs are reported in Table 2, and some representative gel shift assays can be seen in Figure 3.

To provide a measure of the intrinsic affinities of these mimetics for BIV TAR, without competition from lower-affinity nonspecific binding sites as provided by the tRNA, the binding assays were repeated in the absence of tRNA (Table 3). Although several peptidomimetics exhibited high affinity for TAR RNA even in the presence of a large excess of tRNA, suggesting that the interactions are specific, the binding constants are typically lower (tighter binding) by at least 1 order of magnitude in the absence of the tRNA.

Finally, we compared binding of these peptides to BIV TAR with the results for HIV-1 TAR and RRE RNA, to evaluate whether the interactions we observed are specific. Remarkably, very large differences in affinity between BIV and HIV TAR were observed when even single amino acid mutations were introduced. For example, peptides L-02, L-03, and L-09 do not bind to BIV TAR at all, while these peptides bind HIV TAR strongly. Thus, the location of Arg side chains on the hairpin scaffold is an important feature not just of the affinity but also of the selectivity of these peptidomimetics. In contrast, peptides L-66−L-69 bound to HIV TAR weakly compared to BIV TAR (or not at all), emphasizing the fact that position 10 could be occupied by different hydrophobic amino acids and retain binding to BIV TAR, but Ile is the optimal residue. On the other hand, Ile was the only hydrophobic residue to retain affinity against HIV TAR; all other hydrophobic residues abolished binding, while the activity with respect to HIV TAR was retained or even increased with the introduction of charged residues such as Asn and Gln in this position. Finally, significant differences in the binding profile between the two highly similar TAR sites were observed for mutants at the β-turn of the peptide loop (peptides L-22−L-28) and for peptides in which multiple mutations were combined such as L-53−L-58 and L-72−L-80. For example, swapping Gly for Lys in L-22 led to a 10-fold increase in the level of HIV TAR binding, mutating Lys to different residues with L-23−L-28 abolished binding, but binding to BIV was not affected by any of these changes. In contrast to what was observed with HIV TAR, most peptides within the library bound to HIV-1 RRE with comparable affinity, yet the affinities were significantly reduced compared to that for the interaction with the TAR RNAs, suggesting that this conformation is not suitable for inhibition of the Rev−RRE interaction. Thus, this family of β-hairpin mimetics binds with nanomolar affinity and high

Table 1: Sequences of β-Hairpin Mimetics BIV2-1−BIV2-12, with K_d Values (in micromolar) Determined for the Interaction of Each with BIV TAR[a]

mimetic	pos. 1	pos. 2	pos. 3	pos. 4	pos. 5	pos. 6	pos. 7	pos. 8	pos. 9	pos. 10	pos. 11	pos. 12	K_d
BIV2	R	V	R	T	R	G	K	R	R	I	R	V	0.15
BIV2-1	A	V	R	T	R	G	K	R	R	I	R	V	nd[b]
BIV2-2	R	A	R	T	R	G	K	R	R	I	R	V	0.3
BIV2-3	R	V	A	T	R	G	K	R	R	I	R	V	nd[b]
BIV2-4	R	V	R	A	R	G	K	R	R	I	R	V	0.3
BIV2-5	R	V	R	T	A	G	K	R	R	I	R	V	nd[b]
BIV2-7	R	V	R	T	R	G	A	R	R	I	R	V	nd[b]
BIV2-8	R	V	R	T	R	G	K	A	R	I	R	V	nd[b]
BIV2-9	R	V	R	T	R	G	K	R	A	I	R	V	nd[b]
BIV2-10	R	V	R	T	R	G	K	R	R	A	R	V	5
BIV2-11	R	V	R	T	R	G	K	R	R	I	A	V	nd[b]
BIV2-12	R	V	R	T	R	G	K	R	R	I	R	A	5

[a] The amino acid changes from BIV2 are underlined. Note that the side chains of residues 1, 3, 5, 8, 10, and 12 are buried in the complex with TAR RNA. pos. stands for position. [b] No binding detected.

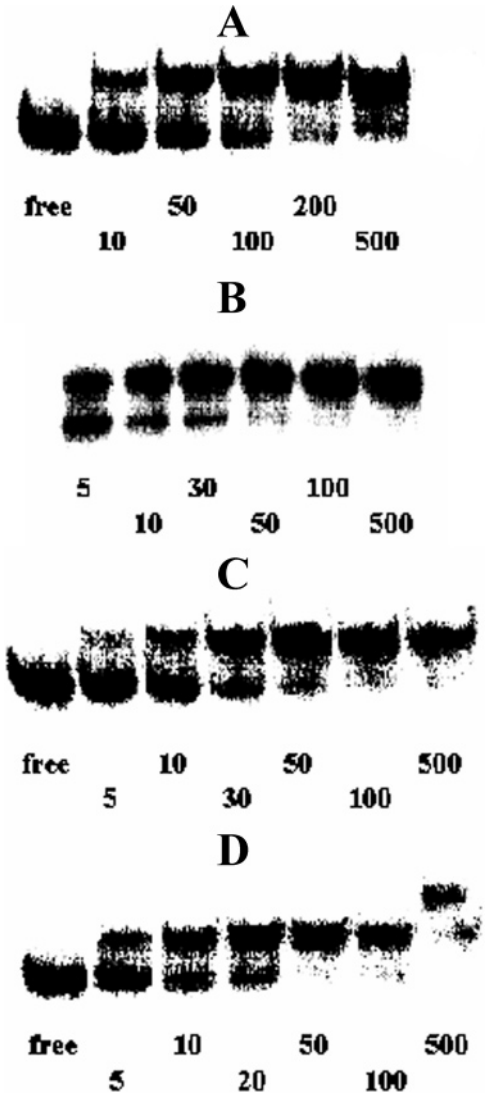

FIGURE 4: Binding of various peptidomimetics to BIV TAR (concentration of 1 nM) in the absence of tRNA: (A) L-57, (B) L-72, (C) L-76, and (D) L-77. Peptide concentrations are in nanomolar.

selectivity to TAR RNAs and discriminates very effectively between the very closely related HIV and BIV structures.

Solution Conformation of the Free Peptidomimetics. The solution conformation of BIV2 was shown earlier to be a stable β-hairpin in aqueous solution (*19*). To verify that the new peptidomimetics retained the same structure, we used NMR to characterize their structure in the absence of RNA. NMR studies on L-42, L-50, and L-51 revealed average β-hairpin structures in solution that are very similar to those deduced earlier for BIV2 for each of the three representative mimetics (data not shown). The NMR structure of mimetic L-22 was studied in more detail (Figure 5), since this has a modified turn sequence at the tip of the hairpin, which might significantly affect the hairpin stability. It is well-known that the turn conformation plays a key role in the formation and stability of hairpin conformations in linear peptides. The structure for L-22 in aqueous solution was determined using 128 NOE upper distance limits (see the Supporting Information). The ensemble of 20 structures (Figure 5) had a backbone rmsd from the average structure of 0.75 ± 0.36 Å (Table 4), indicating a highly structured molecule. While we have not studied the conformation of L-22 bound to BIV TAR, the peptide retains a highly structured conformation and displays the numerous NOEs characteristic of a β-hairpin structure when bound to HIV-1 TAR RNA (data not shown).

Even prior to a formal structure calculation, conclusive evidence for a β-hairpin structure comes from the observation of long-range NOEs between residues on opposite strands of the hairpin, especially Hα−Hα NOEs between non-hydrogen bonding residue pairs and HN−HN NOEs between hydrogen bonding residue pairs on opposite strands (Figure 6). In L-22, Hα−Hα NOEs are observed between Val2 and Arg11 and between Thr4 and Arg9; three HN−HN NOEs involve Arg1−Ile12, Arg3−Ile10, and Arg5−Arg8 connections. Furthermore, cross-strand Hα−HN NOEs were seen between Thr4 and Ile10 and between Val2 and Ile12. The average structures (Figure 5) confirm the predicted stable β-hairpin conformation in which the two strands of the antiparallel β-sheet are connected by a type I′ turn between Lys6 and Gly7, with Lys6 occupying the left-hand region of conformational space.

A semiquantitative estimate of the population of folded structures can be obtained from the intensities of the cross-strand Hα−Hα NOEs, relative to the intensity of the Hα−Hα NOE of Gly7, as a fixed reference distance. However, only the Thr4−Arg9 NOE could be resolved in the D_2O spectra, because the Val2−Arg11 NOE is in the proximity of the diagonal. With reference to the Hα−Hα separation of 2.32 Å found in regular antiparallel β-sheets in proteins (100% folded hairpin), the estimated hairpin population in

Table 2: Sequences of Mutant β-Hairpin Mimetics, with K_d Values (in micromolar) Determined by Electrophoretic Band Shift Assays for the Interaction with BIV TAR[a]

mimetic	pos. 1	pos. 2	pos. 3	pos. 4	pos. 5	pos. 6	pos. 7	pos. 8	pos. 9	pos. 10	pos. 11	pos. 12	K_d
BIV-2	R	V	R	T	R	G	K	R	R	I	R	V	0.15
L-01	**U**	V	R	T	R	G	K	R	R	I	R	**I**	nd
L-02	**K**	V	R	T	R	G	K	R	R	I	R	**I**	nd
L-03	**O**	V	R	T	R	G	K	R	R	I	R	**I**	nd
L-04	**N**	V	R	T	R	G	K	R	R	I	R	**I**	nd
L-05	**Q**	V	R	T	R	G	K	R	R	I	R	**I**	nd
L-06	**Y**	V	R	T	R	G	K	R	R	I	R	**I**	nd
L-07	**L**	V	R	T	R	G	K	R	R	I	R	**I**	nd
L-08	**W**	V	R	T	R	G	K	R	R	I	R	**I**	nd
L-09	R	V	**K**	T	R	G	K	R	R	I	R	V	nd
L-10	R	V	**U**	T	R	G	K	R	R	I	R	V	nd
L-11	R	V	**Q**	T	R	G	K	R	R	I	R	**I**	nd
L-12	R	V	**N**	T	R	G	K	R	R	I	R	**I**	nd
L-13	R	V	R	T	**K**	G	K	R	R	I	R	V	nd
L-14	R	V	R	T	**U**	G	K	R	R	I	R	V	nd
L-15	R	V	R	T	**O**	G	K	R	R	I	R	V	nd
L-16	R	V	R	T	**N**	G	K	R	R	I	R	V	nd
L-17	R	V	R	T	**Q**	G	K	R	R	I	R	V	nd
L-18	R	V	R	T	**I**	G	K	R	R	I	R	V	nd
L-19	R	V	R	T	**L**	G	K	R	R	I	R	V	nd
L-20	R	V	R	T	**Y**	G	K	R	R	I	R	V	nd
L-21	R	V	R	T	R	**N**	**G**	R	R	I	R	**I**	0.5
L-22	R	V	R	T	R	**K**	**G**	R	R	I	R	**I**	0.1
L-23	R	V	R	T	R	G	**R**	R	R	I	R	**I**	~0.3
L-24	R	V	R	T	R	G	**Y**	R	R	I	R	**I**	1
L-25	R	V	R	T	R	G	**Q**	R	R	I	R	**I**	0.5
L-26	R	V	R	T	R	G	**N**	R	R	I	R	**I**	0.2
L-27	R	V	R	T	R	G	**O**	R	R	I	R	**I**	0.2
L-28	R	V	R	T	R	G	**U**	R	R	I	R	**I**	nd
L-29	R	V	R	T	R	G	K	**K**	R	I	R	V	2.5
L-30	R	V	R	T	R	G	K	**U**	R	I	R	V	nd
L-31	R	V	R	T	R	G	K	**O**	R	I	R	V	2.5
L-32	R	V	R	T	R	G	K	**N**	R	I	R	V	nd
L-33	R	V	R	T	R	G	K	**F**	R	I	R	V	nd
L-34	R	V	R	T	R	G	K	**Y**	R	I	R	V	nd
L-35	R	V	R	T	R	G	K	R	**K**	I	R	V	0.15
L-36	R	V	R	T	R	G	K	R	**U**	I	R	V	nd
L-37	R	V	R	T	R	G	K	R	**O**	I	R	V	0.15
L-38	R	V	R	T	R	G	K	R	**N**	I	R	V	nd
L-39	R	V	R	T	R	G	K	R	**Q**	I	R	V	nd
L-40	R	V	R	T	R	G	K	R	R	I	**K**	V	0.15
L-41	R	V	R	T	R	G	K	R	R	I	**U**	V	nd
L-42	R	V	R	T	R	G	K	R	R	I	**O**	V	0.1
L-43	R	V	R	T	R	G	K	R	R	I	**N**	V	5
L-44	R	V	R	T	R	G	K	R	R	I	**Q**	V	nd
L-45	R	V	R	T	R	G	K	R	R	I	R	**L**	0.12
L-46	R	V	R	T	R	G	K	R	R	I	R	**I**	0.10
L-47	R	V	R	T	R	G	K	R	R	I	R	**F**	0.20
L-48	R	V	R	T	R	G	K	R	R	I	R	**T**	~0.12
L-49	R	V	R	T	R	G	K	R	R	I	R	**N**	0.1
L-50	R	V	R	T	R	G	K	R	R	I	R	**R**	0.15
L-51	R	**T**	R	T	R	G	K	R	R	I	R	V	0.05
L-52	R	**N**	R	T	R	G	K	R	R	I	R	V	0.15
L-53	R	**Q**	R	T	R	G	K	R	R	I	R	**I**	0.2
L-54	R	**Y**	R	T	R	G	K	R	R	I	R	**I**	0.2
L-55	R	**W**	R	T	R	G	K	R	R	I	R	**I**	0.5
L-56	R	**L**	R	T	R	G	K	R	R	I	R	**I**	0.2
L-57	R	**T**	R	T	R	G	K	R	R	I	R	**I**	0.05
L-58	R	**N**	R	T	R	G	K	R	R	I	R	**I**	0.1
L-59	R	V	R	**Q**	R	G	K	R	R	I	R	V	0.05
L-60	R	V	R	**V**	R	G	K	R	R	I	R	V	~0.15
L-61	R	V	R	**Y**	R	G	K	R	R	I	R	V	0.1
L-62	R	V	R	**K**	R	G	K	R	R	I	R	V	0.05
L-63	R	V	R	**Q**	R	G	K	R	R	I	R	**I**	0.2
L-64	R	V	R	**V**	R	G	K	R	R	I	R	**I**	0.2
L-65	R	V	R	**Y**	R	G	K	R	R	I	R	**I**	0.2
L-66	R	V	R	T	R	G	K	R	R	**L**	R	V	~0.35
L-67	R	V	R	T	R	G	K	R	R	**X**	R	V	5
L-68	R	V	R	T	R	G	K	R	R	**F**	R	V	0.20
L-69	R	V	R	T	R	G	K	R	R	**Y**	R	V	0.5
L-70	R	V	R	T	R	G	K	R	R	**N**	R	V	~0.3

Table 2: (Continued)

mimetic	pos. 1	pos. 2	pos. 3	pos. 4	pos. 5	pos. 6	pos. 7	pos. 8	pos. 9	pos. 10	pos. 11	pos. 12	K_d
L-71	R	V	R	T	R	G	K	R	R	**Q**	R	V	~0.3
L-72	R	V	R	T	R	G	K	R	R	I	**O**	**I**	0.05
L-73	R	V	R	T	R	G	K	R	R	I	**K**	**I**	0.1
L-74	R	V	R	T	R	G	K	R	**K**	I	**O**	**I**	0.1
L-75	R	**T**	R	**Q**	R	G	K	R	R	I	R	**I**	0.1
L-76	R	**T**	R	T	R	G	K	R	R	I	**O**	**I**	0.05
L-77	R	**T**	R	T	R	G	K	R	**K**	I	**O**	**I**	0.05
L-78	R	**T**	R	**Q**	R	G	K	R	R	I	**O**	**I**	0.05
L-79	R	**T**	R	**V**	R	G	K	R	R	I	**O**	**I**	0.1
L-80	R	**T**	R	**Y**	R	G	K	R	R	I	**O**	**I**	0.1
L-81	R	V	R	T	R	G	K	R	R	**F**	R	**I**	1
L-82	R	**T**	R	T	R	G	K	R	R	**F**	R	**I**	0.5
L-83	R	**T**	R	T	R	G	K	R	R	**F**	**O**	**I**	0.2
L-84	R	V	R	**Q**	R	G	K	R	R	**F**	**O**	**I**	1
L-85	R	**T**	R	**V**	R	G	K	R	**K**	**F**	**O**	**I**	0.5
L-86	R	**T**	R	**Y**	R	G	K	R	**K**	**F**	**O**	**I**	1

[a] The standard one-letter code is used for amino acids except as follows: U for L-citrulline, O for L-ornithine, and X for L-cyclohexylalanine. Note that the side chains of residues 1, 3, 5, 8, 10, and 12 are on the face of the β-hairpin facing the TAR RNA (see Figures 1 and 2). pos. stands for position. [b] No binding detected.

Table 3: K_d Values for Selected Mimetics Binding to TAR RNA, Determined by EMSAs in the Absence of tRNA[a]

mimetic	K_d (μM)	mimetic	K_d (μM)	mimetic	K_d (μM)
BIV2	0.15 (0.15)	L-63	0.02 (0.2)	L-75	0.1 (0.03)
L-22	0.005 (0.1)	L-72	0.005 (0.05)	L-76	0.05 (0.02)
L-46	0.07 (0.1)	L-73	0.005 (0.1)	L-77	0.007 (0.05)
L-57	0.03 (0.05)	L-74	0.01 (0.1)	L-78	0.007 (0.05)

[a] The K_d values found by EMSAs with carrier tRNA present are given in parentheses.

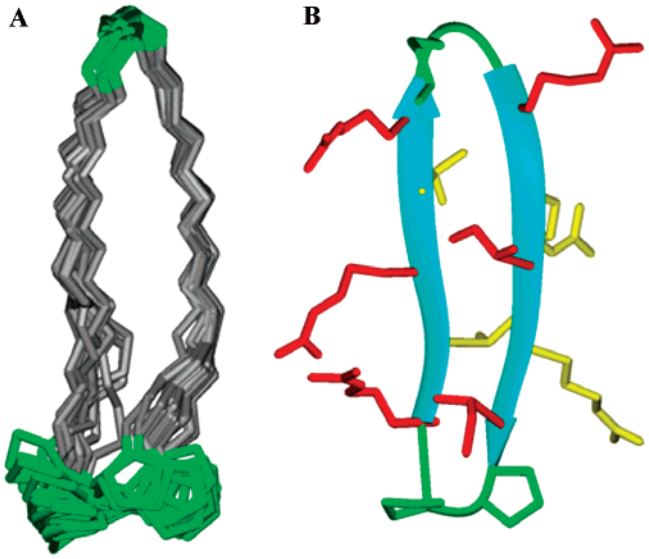

FIGURE 5: (A) Backbone superposition and representation of the final 20 NMR structures for L-22. (B) A typical NMR structure with the ribbon representation (cyan) of the two strands. The β-turns are colored green, the downward-facing (facing the RNA) residues red, and the upward-facing residues (solvent-exposed related to RNA binding) yellow.

Table 4: Experimental Distance Restraints and Statistics for the Final 20 NMR Structures Calculated for L-22

no. of NOE upper distance limits	128
no. of intraresidue limits	56
no. of sequential limits	59
no. of medium- and longe-range limits	23
residual target function value (Å^2)	0.44 ± 0.05
mean rmsd values (Å)	
all backbone atoms	0.75 ± 0.36
all heavy atoms	2.50 ± 0.65
residual NOE violation	
no. >0.2 Å	none
maximum (Å)	none

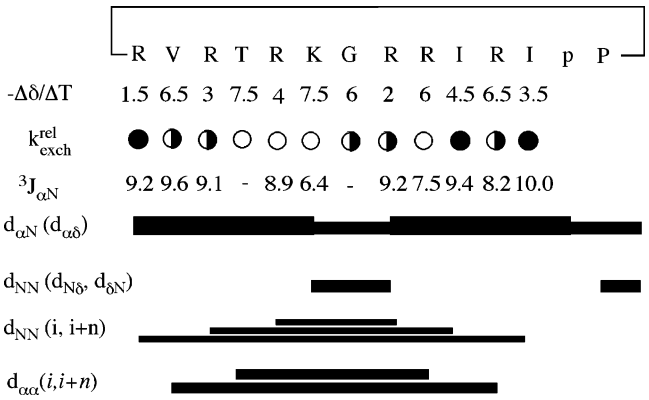

FIGURE 6: HN temperature coefficients (in parts per billion per kelvin) determined over the range of 278−314 K. Relative H−D exchange rates of peptide amide protons (black circles, slow; half-white circles, medium; and white circles, fast), backbone $^3J_{\alpha N}$ coupling constants determined with one-dimensional spectra, and characteristic backbone NOE connectivities (thick line, strong; medium line, medium; and thin line, weak) measured for L-22.

L-22 is then ~90%. Another method of estimating folded β-structures makes use of the $\alpha N(i,i+1)/\alpha N(i,I)$ NOE intensity ratio. Values of ~2.3 correlate with random coil conformations, whereas larger values of ~8 are predicted for an ideal antiparallel β-sheet. The intensity ratios for residues in the predicted β-strands of L-22 (1−5 and 8−11) are in the range of 4.4−11.4 and thus provide further support for highly populated β-conformations. The intensity ratio of <1 for the same pair of NOEs observed for Lys6 and Gly7 is consistent with the left-handed (α_L) population in a type I′ turn. The predominant occurrence of the type I′ β-turn, with the atypical left-handed helical orientation of Lys6, is confirmed by characteristic NOE connectivities, in particular, by the sequential HN−HN (Lys6−Gly7 and Gly7−Arg8) and Hα−HN (Lys6−Arg8) NOEs, as well as the strong intramolecular Hα−HN NOEs of Lys6 and Gly7.

The temperature dependence of amide proton chemical shifts, as well as relative H−D exchange rates, provides

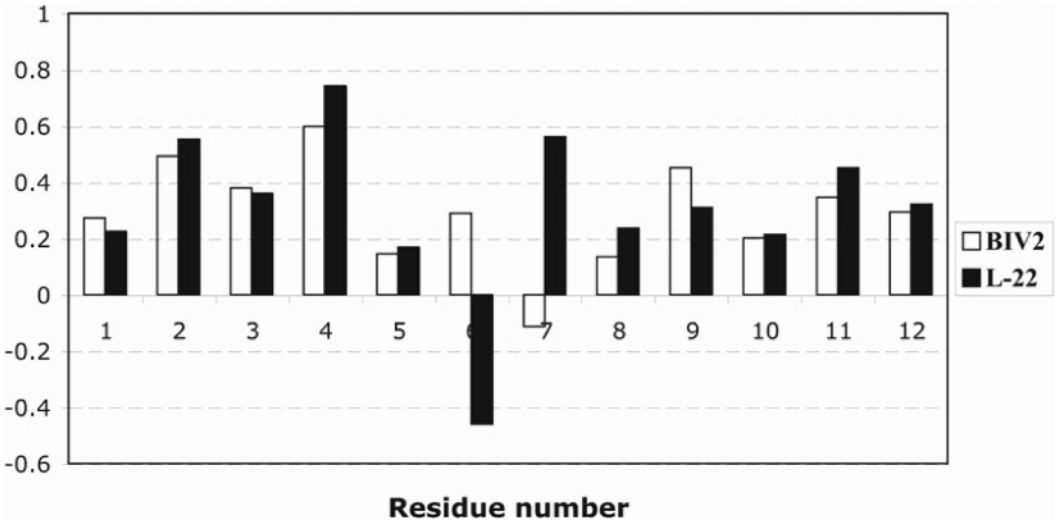

FIGURE 7: Hα chemical shifts relative to random coil chemical shifts of residues in peptidomimetics BIV2 (white) and L-22 (black).

complementary information about the involvement of amide NH groups in hydrogen bonding and/or their solvent accessibility. Relatively small temperature coefficients (Figure 6) were observed for Arg1, Arg3, Arg5, Arg8, Ile10, and Ile12, as expected for residues in cross-strand hydrogen bonding positions. The relative H−D exchange rates of amide NHs are significantly slowed for Arg1, Arg3, and in particular Ile10 and Ile12. The very slow exchange rates of Ile10 (half-life, $t_{1/2} = 32$ h) and Ile12 ($t_{1/2} = 13$ h) NH groups might be due not only to their involvement in cross-strand hydrogen bonding but also to shielding from the solvent by their aliphatic side chains.

Finally, $^3J_{\alpha N}$ coupling constants are correlated with the backbone torsion angle ϕ via the Karplus equation. Coupling constants of >8.5 Hz should be observed in the case of extended torsion angles (ϕ) as they occur in β-sheets. In L-22, the coupling constants of residues in the β-strands show predominantly those larger values typical of β-structure (Figure 6). The differences between the CαH chemical shift values determined experimentally and the random coil values are also widely used as an indicator of secondary structure formation (*32*, *33*). Downfield shifts of Hα by >0.1 ppm ($\Delta\delta$), which are indicative of residues in an extended β-sheet conformation (*34*, *35*), are observed for residues 1−5 and 8−12 in BIV2 and L-22 (Figure 7).

DISCUSSION

We have recently described the discovery of BIV2 (Figure 1) (*19*), a conformationally constrained mimetic of BIV Tat that inhibited the Tat−TAR interaction in this lentivirus. Although peptidomimetic inhibitors of the Tat−TAR interaction have been described in the past, previous studies used flexible linear mimetics such as peptoids (*10*) or oligocarbamates (*36*). Through the introduction of the D-Pro-L-Pro template, we wanted to generate a structurally rigid mimetic, and through cyclization, we wanted to stabilize the peptide against proteolysis. In studying a small library of mimetics (*19*), we demonstrated that formation of the desired structure was required for binding and that even small changes in the peptide sequence led to large changes in affinity. In contrast, previous linear peptidomimetic structures were insensitive to even significant changes in their sequence, indicating a nonspecific interaction and making it very difficult to provide suggestions for improving activity.

BIV2 binds to BIV TAR with a dissociation constant (K_d) of 150 nM, when measured in the presence of a 10000-fold excess of tRNA. NMR showed that it adopts a β-hairpin backbone conformation, both free in solution (*19*) and in the complex with TAR (*25*). Thus, the structure of the free peptidomimetic is effectively pre-organized for binding to the RNA, as we had hypothesized in the design of the peptidomimetic library. Surprisingly, however, the orientation of bound BIV2 was flipped head to tail compared to what was expected (*19*) on the basis of the design of the mimetic and the bound orientation of the BIV Tat peptide. Thus, in the Tat−TAR structure, the N- and C-termini of the peptide are oriented toward the tip of the RNA hairpin. These termini are mimicked by residues directly attached to the D-Pro-L-Pro hairpin-stabilizing template in BIV2, which are now oriented away from the tip of the RNA (Figure 2). Nevertheless, both the Tat peptide and BIV2 bind in such a way that it is mostly residues on one face of their respective β-hairpin structures that contact the RNA, while side chains on the opposite face are oriented toward the solution (Figures 1 and 2). For BIV2, the side chains at positions 1, 3, 5, 8, 10, and 12 interact with the major groove of the RNA, whereas residues 2, 4, 9, and 11 on the other face are exposed to solvent. Residues 6 and 7 at the tip of the BIV2 β-hairpin point toward the tip of the RNA. When examined more closely, three Arg side chains are buried in the interface in very similar positions in both complexes. These are Arg70, Arg73, and Arg77 in BIV Tat (Tat numbering) and Arg3, Arg1, and Arg5 in BIV2. The positional overlap of Arg3 with Arg70 and Arg1 with Arg73 in the superimposed complexes is remarkable, but the guanidinium groups of Arg5 and Arg77 are farther apart (Figure 2). This mimicry is all the more interesting since Arg1, Arg3, and Arg5 in BIV2 are found along one strand of the hairpin whereas Arg70, Arg73, and Arg77 in Tat are located in both strands.

These results provided us with the opportunity to use rational methods to optimize the activity of the peptide, thus demonstrating that this class of peptidomimetic inhibitors is both potent and specific. While it has been possible in the past to discover small molecule nanomolar inhibitors of the

Tat−TAR interaction in HIV, specificity has been difficult to obtain. In this work, we demonstrate that just a few rounds of optimization led to the discovery of nanomolar inhibitors of the BIV Tat−TAR interaction; remarkably, the inhibitors are strongly selective over a structure as closely related as HIV-1 TAR, demonstrating that the structural rigidity imposed by the template provides selectivity by locking the pharmacophore in a defined location at the peptide−RNA interface.

Mutagenesis studies (*37*) of the Tat protein revealed that Arg70, Gly71, Arg73, Gly74, Arg77, and Ile79 are energetically most important for binding to TAR. When considering the binding data with BIV2 variants [first from the alanine scanning library (Table 1)], we observed that substituting any one of the cationic residues with alanine has large destabilizing effects on TAR binding. We were surprised to observe that this was the case even for Arg9 and Arg11 that are on the solvent-exposed face of the hairpin in the BIV2−TAR complex. This may be due to the loss of key electrostatic interactions with the phosphate groups in the RNA backbone, a conclusion that is supported by studies of other mutants (vide infra).

More detailed insight into the determinants of affinity and specificity comes from analysis of the large library of BIV2 variants (Table 2). This library was not made and screened in a single step, but rather in a stepwise manner. The information obtained from screening a first set of mimetics was used in designing later variants. Although the library is relatively large, it represents a small fraction of the total sequence space potentially available to these peptides; we were obviously limited in the total number of molecules that could be made and tested, which limited in turn the number of variants studied at each position. Ile was frequently incorporated at position 12 throughout the library, since it quickly became apparent that the Val12Ile change consistently gave a small improvement in affinity. However, it is interesting that Val12 (which points into the major groove of TAR) could also be replaced with polar and even aromatic residues, such as Asn, Thr, or Phe [L-45−L-50 (Table 2)], with only small changes in activity. Truncating the side chain to Ala (Table 1), however, led to a much greater loss of affinity. The Val12Ala change might also influence the conformational properties of the ligand, which would affect binding affinity in a way that is difficult to estimate.

With regard to the cationic residues in BIV2, the key roles of the Arg1, Arg3, and Arg5 side chains (indicated by the Ala scanning mutants) are reinforced by the fact that all the substitutions that were tested [L-01−L-20 (Table 2)] at these positions abolished binding to the RNA, including lysine and ornithine. These results suggest that both the positive charge and the specific hydrogen bonding abilities of the guandinium groups are important for tight binding. In the BIV2−TAR complex, Arg1, Arg3, and Arg5 side chains are buried in the RNA major groove, and all three guanidinium groups are located in positions where strong hydrogen bonding with base pairs and/or the RNA backbone occurs. We were pleased to observe clear differences at these positions when we compared binding of these peptides to HIV and BIV TAR, strongly suggesting that the interaction is highly specific because these two structures are very closely related.

The tip of the hairpin in BIV2 is a β-turn formed by Gly6 and Lys7. The lysine side chain does not contact the RNA in the complex but rather points out into solution. Consistent with this observation, a number of substitutions of Lys7 were tolerated well [L-21−L-28 (Table 2)] and reversing the order to Lys6 and Gly7 (L-22) had no significant impact on the affinity for TAR RNA (L-22 vs L-46). Models of the complex suggest that this Lys side chain in mutant L-22 would also be directed into solution. This is in clear contrast to the binding of these mutants against HIV TAR; for example, L-22 binds with a 10-fold increase in activity compared to BIV2, and any mutation of Lys at position 7 (peptides L-23−L-28) abolished binding.

The solution conformation of free L-22 was investigated by NMR spectroscopy, as a representative high-affinity ligand. Reassuringly, the peptide was shown to form a very stable β-hairpin conformation despite the change at the hairpin tip. In complex with HIV TAR, the same peptide retains the NMR signature of a highly structured peptide, almost certainly a β-hairpin; we have not, however, investigated its conformation when bound to BIV TAR. Thermodynamic studies of hairpin stability in other model peptides frequently highlight the stabilizing effects of cross-strand aromatic−aromatic interactions (*38*), which clearly are not relevant here. It seems likely, however, that cross-strand hydrophobic interactions may help stabilize the hairpin conformation in both free and RNA-bound L-22. Thus, the hydrophobic methylene groups within the Arg side chains always lie across the hairpin and are in contact with aliphatic groups (Arg1−Ile12, Val2−Arg11, Arg3−Ile10, and Thr4−Arg9). These hydrophobic interactions, together with an especially stable type I′ β-turn sequence (Lys6-Gly7 is a turn type that matches the natural left-handed twist of a β-hairpin), most likely account for the high hairpin stability.

The guanidinium group of Arg8 contacts the base pairs at the tip of the RNA hairpin but is not buried in the structure of the complex. At this position, neutral replacements [L-29−L-34 (Table 2)] were not tolerated, but Lys and Orn mutants still bind the RNA, although with a more than 1 order of magnitude weaker affinity. Thus, the positively charged nature of the side chain appears to play a more important role in binding, while the specific hydrogen bonding ability of the guandinium group is less important. In contrast, Arg8 to Lys/Orn mutants retained activity against HIV TAR. It is clear from Table 2 that similar considerations for BIV apply to Arg9 and Arg11 as well (L-35−L-44), although these side chains are directed away from the RNA into solution. Indeed, the Lys and Orn replacements at these positions yield full activity for BIV TAR with respect to BIV2.

The side chain of Val2 is on the solvent-exposed side of the mimetic in the complex. It contacts the methylene groups in the side chain of Arg11 on the opposite β-strand of the mimetic but does not contact the RNA. Consistent with this result, the data in Table 2 (L-51−L-58) show that a variety of different side chains are tolerated here, without a large loss (or gain) in affinity. The Val2Thr change does, however, yield a small improvement in binding affinity for BIV TAR, possibly since Thr is at once similar in size and shape to Val but also contains a more polar group for interaction with water on this solvent-exposed face of the complex. When we combined mutations at positions 2 and 12 (peptides L-51−L-58), binding to BIV TAR was unaffected while binding to HIV TAR was lost. A similar situation occurs with Thr4, which is also solvent-exposed and does not

contact the RNA. A variety of different side chains are tolerated here [L-59−L-65 (Table 2)], and in one case, Thr4Gln, a small increase in affinity for BIV TAR is seen. When both Val2Thr and Thr4Gln changes were introduced, however (mutant L-76), no significant further gain in affinity was noticed, suggesting that the effects of the single changes were not additive; furthermore, combined mutations at these positions totally abolished binding to HIV TAR.

The final series of single-point changes were at position Ile10 (L-66−L-71). This side chain is buried in the complex, where it contacts bases in the RNA. As reported for Ile79 in the native protein (*37*), other hydrophobic residues can maintain the hydrophobic contacts at the RNA−peptide interface but the Ile side chain is optimal, while for HIV TAR, Asn and Gln residues make optimal contacts at position 10. The remaining entries in Table 2 (L-72−L-86) seek additive effects from multiple substitutions, and several mutants exhibited affinities for TAR RNA that were improved compared to those of BIV2.

The binding constants obtained in the presence of tRNA actually represent a complex partition experiment for the peptides between BIV TAR and a much larger excess of tRNA. When we measured the affinities of several mimetics for TAR RNA in the absence of tRNA, the results showed that the K_d for BIV2 was unaltered, yet many of the mutants, for example, L-22, L-72, L-76, and L-77 (Figure 4 and Table 3), exhibited an increase in activity of 1 or even 2 orders of magnitude, in the absence of tRNA. Interestingly, when peptides L-72−L-86 were tested for binding to HIV TAR, affinity was abolished in most cases. In other words, while small additive effects in activity were observed for multiple favorable mutations with BIV TAR, the same was not true for binding of the same peptidomimetics to HIV TAR.

We have demonstrated that peptidomimetic chemistry based on structure-promoting scaffolds yields nanomolar inhibitors of viral protein−RNA interactions. In addition to being as potent as the complete Tat protein they were intended to mimic, these peptides are remarkably specific. Mutations that proved to be most favorable for BIV TAR were not identical to those that led to optimal activity against HIV TAR, and vice versa; single and multiple substitutions allow the peptidomimetics to distinguish between two RNAs that are closely related in structure and sequence. The knowledge generated from the structural analysis and implemented in just a few cycles of design and testing led to a 100-fold improvement in activity compared to that of the lead molecule BIV2. The insight gained through this work into the origins of the affinity and selectivity of binding of peptidomimetics to BIV TAR has recently been exploited in the development of related mimetics that bind tightly to HIV TAR RNA and are highly selective in inhibiting viral replication by a Tat-dependent mechanism.

SUPPORTING INFORMATION AVAILABLE

Relevant analytical data for the L-01−L-86 library (sequence of 12 residues attached to the D-Pro-L-Pro template), including calculated molecular weights (MW_{calc}), masses (m/z) observed by ES-MS, and retention times (t_R) observed by HPLC; chemical shift assignments for peptidomimetic L-22; and a complete list of NOE-derived distance restraints used for L-22 structure calculation. This material is available free of charge via the Internet at http://pubs.acs.org.

REFERENCES

1. Gallego, J., and Varani, G. (2001) Targeting RNA with small molecule drugs: Therapeutic promises and chemical challenges, *Acc. Chem. Res. 34*, 836−843.
2. Arzumanov, A., Walsh, A. P., Rajwanshi, V. K., Kumar, R., Wengel, J., and Gait, M. J. (2001) Inhibition of HIV-1 Tat transactivation by steric block chimeric 2′-O-methyl/LNA oligoribonucleotides, *Biochemistry 40*, 14645−14654.
3. Arzumanov, A., Walsh, A. P., Liu, X., Rajwanshi, V. K., Wengel, J., and Gait, M. J. (2001) Oligonucleotide analogue interference with the HIV-1 Tat protein TAR RNA interaction, *Nucleosides, Nucleotides Nucleic Acids 20*, 471−480.
4. Lee, N. S., Dohjima, T., Bauer, G., Li, H. T., Li, M. J., Ehsani, A., Salvaterra, P., and Rossi, J. (2002) Expression of small interfering RNAs targeted against HIV-1 rev transcripts in human cells, *Nat. Biotechnol. 20*, 500−505.
5. Surabhi, R. M., and Gaynor, R. B. (2002) RNA interference directed against viral and cellular targets inhibits human immunodeficiency virus type 1 replication, *J. Virol. 76*, 12963−12973.
6. Cundliffe, E., and Thompson, J. (1981) Concerning the mode of action of micrococcin upon bacterial protein synthesis, *Eur. J. Biochem. 118*, 47−52.
7. Wang, S., Huber, P. W., Cui, M., Czarnik, A. W., and Mei, H.-Y. (1998) Binding of neomycin to TAR element of HIV-1 RNA induces dissociation of Tat protein by an allosteric mechanism, *Biochemistry 37*, 5549−5557.
8. Keen, N. J., Gait, M. J., and Karn, J. (1996) Human immunodeficiency virus type-1 Tat is an integral component of the activated transcription-elongation complex, *Proc. Natl. Acad. Sci. U.S.A. 93*, 2505−2510.
9. Karn, J. (1999) Tackling Tat, *J. Mol. Biol. 293*, 235−254.
10. Hamy, F., Felder, E. R., Heizmann, G., Lazdins, J., Aboul-ela, F., Varani, G., Karn, J., and Klimkait, T. (1997) An inhibitor of the Tat/TAR RNA interaction that effectively suppresses HIV-1 replication, *Proc. Natl. Acad. Sci. U.S.A. 94*, 3548−3553.
11. Hamy, F., Brondani, V., Flörsheimer, A., Stark, W., Blommers, M. J. J., and Klimkait, T. (1998) A new class of HIV-1 Tat antagonist acting through Tat-TAR inhibition, *Biochemistry 37*, 5086−5095.
12. Mei, H.-Y., Galan, A. A., Halim, N. S., Mack, D. P., Moreland, D. W., Sanders, K. B., Truong, H. N., and Czarnik, A. W. (1995) Inhibition of an HIV-1 Tat-derived peptide binding to TAR RNA by aminoglycoside antibiotics, *Bioorg. Med. Chem. Lett. 22*, 2755−2760.
13. West, M. J., Lowe, A. D., and Karn, J. (2001) Activation of human immunodeficiency virus transcription in T cells revisited: NF-κB p65 stimulates transcriptional elongation, *J. Virol. 75*, 8524−8537.
14. Williams, S. A., Chen, L. F., Kwon, H., Ruiz-Jarabo, C. M., Verdin, E., and Greene, W. C. (2006) NF-κB p50 promotes HIV latency through HDAC recruitment and repression of transcriptional initiation, *EMBO J. 25*, 139−149.
15. Krebs, A., Ludwig, V., Boden, O., and Gobel, M. W. (2003) Targeting the HIV trans-activation responsive region? Approaches towards RNA binding drugs, *ChemBioChem 6*, 972−978.
16. Gadek, T. R., Burdick, D. J., McDowell, R. S., Stanley, M. S., Marsters, J. C., Jr., Paris, K. J., Oare, D. A., Reynolds, M. E., Ladner, C., Zioncheck, K. A., Lee, W. P., Gribling, P., Dennis, M. S., Skelton, N. J., Tumas, D. B., Clark, K. R., Keating, S. M., Beresini, M. H., Tilley, J. W., Presta, L. G., and Bodary, S. C. (2002) Generation of an LFA-1 antagonist by the transfer of the ICAM-1 immunoregulatory epitope to a small molecule, *Science 295*, 1086−1093.
17. Gadek, T. R., and McDowell, R. S. (2003) Discovery of small molecule leads in a biotechnology datastream, *Drug Discovery Today 8*, 545−550.
18. Tamilarasu, N., Huq, I., and Rana, T. M. (2001) Targeting RNA with peptidomimetic oligomers in human cells, *Bioorg. Med. Chem. Lett. 11*, 505−507.
19. Athanassiou, Z., Dias, R. L. A., Moehle, K., Dobson, N., Varani, G., and Robinson, J. A. (2004) Structural mimicry of retroviral Tat proteins by constrained β-hairpin peptidomimetics: Ligands with high affinity and selectivity for viral RNA regulatory elements, *J. Am. Chem. Soc. 126*, 6906−6913.

20. Aboul-ela, F., Karn, J., and Varani, G. (1995) The structure of the human immunodeficiency virus type-1 TAR RNA reveals principles of RNA recognition by Tat protein, *J. Mol. Biol. 253*, 313−332.
21. Aboul-ela, F., Karn, J., and Varani, G. (1996) Structure of HIV-1 TAR RNA in the absence of ligands reveals a novel conformation of the trinucleotide bulge, *Nucleic Acids Res. 24*, 3974−3981.
22. Puglisi, J. D., Chen, L., Frankel, A. D., and Williamson, J. R. (1993) Role of RNA structure in arginine recognition of TAR RNA, *Proc. Natl. Acad. Sci. U.S.A. 90*, 3680−3684.
23. Puglisi, J. D., Chen, L., Blanchard, S., and Frankel, A. D. (1995) Solution structure of a bovine immunodeficiency virus Tat-TAR peptide-RNA complex, *Science 270*, 1200−1203.
24. Ye, X., Kumar, R. A., and Patel, D. J. (1995) Molecular recognition in the bovine immunodeficiency virus Tat peptide-TAR RNA interaction, *Chem. Biol. 2*, 827−840.
25. Leeper, T. C., Athanassiou, Z., Dias, R. L. A., Robinson, J. A., and Varani, G. (2005) TAR RNA recognition by a cyclic peptidomimetic of Tat protein, *Biochemistry 44*, 12362−12372.
26. Gills, S. C., and von Hippel, P. H. (1989) Calculation of protein extinction coefficients from amino acid sequence data, *Anal. Biochem. 182*, 319−326.
27. Atherton, E., and Sheppard, R. C. (1989) *Solid Phase Peptide Synthesis: A practical Approach*, IRL Press, Oxford, U.K.
28. Milligan, J. (1987) Oligoribonucleotide synthesis using T7 RNA polymerase and synthetic DNA templates, *Nucleic Acids Res. 15*, 8733−8798.
29. Bartels, C., Xia, T.-h., Billeter, M., Güntert, P., and Wüthrich, K. (1995) The program XEASY for computer-supported NMR spectral analyis of biological macromolecules, *J. Biomol. NMR 6*, 1−10.
30. Guntert, P., Mumenthale, C., and Wuthrich, K. (1997) Torsion angle dynamics for NMR structure calculation with the new program DYANA, *J. Mol. Biol. 273*, 283−298.
31. Koradi, R., Billeter, M., and Wuthrich, K. (1996) MOLMOL: A program for display and analysis of macromolecular structures, *J. Mol. Graphics 14*, 51−55.
32. Griffiths-Jones, S. R., Maynard, A. J., and Searle, M. S. (1999) Dissecting the stability of a β-hairpin peptide that folds in water: NMR and molecular dynamics analysis of the β-turn and β-strand contributions to folding, *J. Mol. Biol. 292*, 1051−1069.
33. Maynard, A. J., Sharman, G. J., and Searle, M. S. (1998) Origin of β-hairpin stability in solution: Structural and thermodynamic analysis of the folding of a model peptide supports hydrophobic stabilization in water, *J. Am. Chem. Soc. 120*, 1996−2007.
34. Wishart, D. S., Sykes, B. D., and Richards, F. M. (1991) Relationship between nuclear magnetic resonance chemical shift and protein secondary structure, *J. Mol. Biol. 222*, 311−333.
35. Wishart, D. S., Sykes, B. D., and Richards, F. M. (1992) The chemical shift index: A fast and simple method for the assignment of protein secondary structure through NMR spectroscopy, *Biochemistry 31*, 1647−1651.
36. Hwang, S., Tamilarasu, N., Kibler, K., Cao, H., Ali, A. m., Ping, Y., Jeang, K., and Rana, T. (2003) Discovery of a small molecule Tat-TAR RNA antagonist that potently inhibits HIV-1 replication, *J. Biol. Chem. 40*, 39092−39103.
37. Chen, L., and Frankel, A. D. (1995) A peptide interaction in the major groove of RNA resembles protein interactions in the minor groove of DNA, *Proc. Natl. Acad. Sci. U.S.A. 92*, 5077−5081.
38. Searle, M. S., and Ciani, B. (2004) Design of β-sheet systems for understanding the thermodynamics and kinetics of protein folding, *Curr. Opin. Struct. Biol. 14*, 458−464.

BI0619371